Physica A 530 (2019) 121543

Contents lists available at ScienceDirect

Physica A

journal homepage: www.elsevier.com/locate/physa

Multichannel Complexity Index (MCI) for a multi-organ physiological complexity assessment

Mimma Nardelli *, Enzo Pasquale Scilingo, Gaetano Valenza

Bioengineering and Robotics Research Centre E. Piaggio & Department of Information Engineering, University of Pisa, Italy

HIGHLIGHTS

- An algorithm for the Multichannel Complexity Index computation is described.
- The algorithm was validated using synthetic series and real physiological data.
- MCI performance was compared with state of the art multivariate entropy metrics.
- MCI may be linked to coupled dynamics between sub-systems

ARTICLE INFO

Article history:
Received 26 September 2018
Received in revised form 8 April 2019
Available online 30 May 2019

Keywords:
Complexity
Multivariate multiscale entropy
Fuzzy entropy
Autonomic nervous system
Heart rate variability
Blood pressure
Synthetic series
Fantasia database
Tilt table test

ABSTRACT

Quantitative measurements of multi-organ interplay are crucial for the assessment of multivariate physiological dynamics in health and disease. Nevertheless, current quantification of multivariate complexity for nonlinear physiological processes is limited by reliability issues on short-time series, and parameters sensitivity especially in case of a multiscale analysis. To overcome these limitations, we propose a new tool to characterize the complexity of interacting physiological processes that may have different temporal dynamics: the Multichannel Complexity Index (MCI). This metrics relies on a novel method for the reconstruction of the multivariate phase space, where each series is embedded using its proper time delay. MCI accounts for the estimation of phase space distances using fuzzy rules, and may be computed at two different ranges of time-scale values to investigate short- and long-term dynamics. We validated our algorithm using three-channel white gaussian noise and 1/f noise systems, with different levels of coupling. By applying our approach to these data, we demonstrate that the MCI method allows to discern not only the degree of complexity in the system dynamics, but also the across-channel coupling level. Results on synthetic series from the Henón map and Rössler attractor demonstrate that MCI effectively discerns between different dynamical behaviours, outperforming state of the art metrics such as the Refined Composite Multivariate Multiscale Fuzzy Entropy. On publicly-available physiological series, considering heartbeat dynamics and blood pressure variability, results demonstrate a MCI sensitivity to postural changes($p < 10^{-2}$ for rest vs. slow-tilt, and $p < 0.05$ for rest vs. rapid-tilt/stand-up conditions), as well as a MCI sensitivity to subjects' age-range (data gathered while watching *Fantasia* Disney movie, 1940) with $p < 10^{-2}$ for short scales and $p = 0.03$ for long scales. In conclusion, MCI is a viable tool for an effective multivariate physiological complexity assessment. The Matlab code implementing the proposed MCI algorithm is available online.

* Corresponding author.
E-mail address: m.nardelli@ing.unipi.it (M. Nardelli).

https://doi.org/10.1016/j.physa.2019.121543
0378-4371/

1. Introduction

Complex physiological systems are characterized by nonlinear dynamics interacting with other systems or subcomponents, such that the system as a whole shows behaviours that the individual components acting alone cannot [1–6].

The cardiovascular system and associated autonomic nervous system (ANS) control can be considered as exemplary complex physiological systems, which also show multivariate and multiscale dynamics [1,3–5,7]. In fact, it is known since 1969 that the cardiovascular system is constantly involved in a dynamical, mutual interplay with numerous other physiological subsystems (e.g., endocrine, neural, and respiratory), as well as in multiple self-regulating, adaptive biochemical processes [8]. In this context, the effects of combined sympathetic and vagal stimulation on heart rate, as controlled by the so-called central autonomic network [9] are not simply additive. Therefore, measures of multivariate nonlinear/complex physiological dynamics are needed.

Previous studies widely investigated univariate physiological complexity especially using entropy and other phase-space derived metrics, including e.g. Lyapunov exponents, for the assessment of cardiovascular and brain dynamics [1,3,4,7,10–14].

Note that, considering Heart Rate Variability (HRV) series, such studies consistently reported on a complexity decrease associated with sympatho-vagal unbalancing due to postural changes [15], as well as a complexity decrease associated with ageing [1,16] (although contradictory findings have also been reported [17,18]).

As entropy increases with the degree of randomness in physiological dynamics, a multiscale entropy approach has been proposed in [5], and further refined in [19]. This approach accounts for the inherent information in physiological dynamics observed at different time-scale resolutions, improving on the discrimination of health and disease states [5,20–22]. Note that previous studies in patients with heart failure suggested that heartbeat scaling and multifractal properties are not generated at the sinus node level, but rather by the intrinsic action of a short-term vagal control and of sympatho-vagal fluctuations associated with the circadian cardiovascular activity especially within the very low frequency band [23].

As the majority of studies dealing with physiological nonlinearity and complexity accounted for a univariate assessment [1,3–5], they neglected most of the multivariate, nonlinear/complex information underlying multi-organ interplay. Taking advantage from multichannel non-invasive recordings of ANS and cardiovascular dynamics, a multivariate version of multiscale entropy has been proposed [24–27]. Indeed, when the variables measured from the same system are not independent and their dynamics are characterized by coupling and loops, the multivariate approaches can be crucial for reconstructing the underlying pathophysiological dynamics [25]. Note that such a multivariate assessment outperformed the standard, univariate complexity assessment in discerning physiological dynamics from elderly vs. young subjects [24,25].

In this study we propose a novel algorithm for the investigation of multivariate-multiscale entropy in patho-physiology: Multichannel Complexity Index (MCI). This approach includes a novel estimation of the multivariate phase space. The choice of time delay and embedding dimension is a crucial point for a phase space reconstruction, as arbitrary values may lead to misleading results [13,28–30] especially for short-time series [31]. In a standard approach, the embedding dimension of a multivariate phase space is equal to the sum of the embedding dimensions associated with each single channel [25]. Recent studies proposed different approaches to optimize such a parameter choice in a multichannel analyses [31–33]. In this study, we estimate specific values of τ and m for each time series of the multivariate process using a mutual correlation function and a false nearest neighbours (FNN) approach, respectively. Then, we exploit these parameters to reconstruct the embedded vectors of the multivariate phase space. Particularly, the information given by univariate embedding vectors is effectively merged into a unique dynamical vector representing the whole state of the system, taking also advantages from a Fuzzy-based computation [34]. This overcomes the limitations of previously proposed approaches regarding the dependence from threshold parameters (e.g., the radius used to identify the neighbour embedded vectors).

The proposed MCI approach is here validated in bivariate and trivariate systems on synthetic and real physiological series. In accordance with the validation procedure that was proposed for other complexity indices [5,25,26], we tested the MCI performance in discerning the systems dynamics in case of white gaussian noise (WGN) and 1/f noise as input, also considering different coupling magnitude. Furthermore, we tested our approach on bivariate Henón map and a trivariate Rössler attractor [12,35–37], including both deterministic and stochastic terms. On real physiological series, we investigated MCI trends from HRV and blood pressure variability series gathered from healthy subjects undergoing postural changes [15,38], as well as young and elderly subjects in a supine position watching Fantasia movie (Disney, 1940) [39,40]. Both datasets were retrieved from the public source: Physionet (http://www.physionet.org/) [39].

Performance of MCI were compared with state of the art multivariate complexity metrics as the Refined Composite Multivariate Multiscale Fuzzy Entropy (RCmvMFE) [26]. RCmvMFE employs a refined composite technique for the coarse-graining of multi-channel time series extending the previous method suggested for univariate signals [41]. Note that RCmvMFE algorithm also uses a fuzzy membership function to estimate similarity of embedded phase space vectors [26].

Preliminary results from this study are in [42].

Synthetic series generation and real experimental protocols are described in Section 2, together with the proposed MCI algorithm and the statistical analysis methods. Results are reported in Section 3, and Discussion and Conclusions follow in Section 4.

2. Materials and methods

2.1. The proposed Multichannel Complexity Index (MCI)

The proposed MCI approach begins with an estimation of the time delay τ, which is the lag at which the time series has to be plotted against itself to reconstruct the phase space, and the embedding dimension m, which corresponds to the phase space dimension. Values of τ and m are estimated for each time series of the multivariate process under study by computing at first the mutual information function and the fraction of the false nearest neighbours (FNN) as a function of the embedding dimension [43]. The integer nearest to the first local minimum of the mutual information function is chosen as τ [44].

As a multiscale approach, the proposed MCI foresees a scaling procedure of the multivariate physiological process, whose amplitudes are normalized using z-score method prior to the coarse-graining implementation. The coarse-grained time series are constructed from the original series by averaging the data points within non-overlapping windows: given a c-variate time series $\mathbf{Y} = \{y_{n,b}\}_{b=1}^{L}$, where $n = 1, \ldots, c$, with L as the length of the series, each element of the coarse-grained series ${}^{\mu}\chi_{n,i}^{(\beta)}$ at scale β is computed as:

$$\begin{aligned} {}^{\mu}\chi_{n,i}^{(\beta)} &= \frac{1}{\beta} \sum_{b=(i-1)\beta+1}^{i\beta} y_{n,b} \\ where \quad 1 \le i \le \left\lfloor \frac{L}{\beta} \right\rfloor &= N, \quad 1 \le n \le c \end{aligned} \tag{1}$$

For each coarse-grained series, the number of samples is equal to the length of the original time series divided by β. Then, at each scale β, the proposed MCI procedure comprises the following steps.

First, considering the embedding dimensions $[m_1, m_2, \ldots, m_c]$ and the time delays $[\tau_1, \tau_2, \ldots, \tau_c]$ of the c-variate process, the MCI multivariate embedded vectors $Z_{\mathbf{M}}$ are defined as follows:

$$\begin{aligned} Z_{\mathbf{M}}(i) = &[\Xi(\chi_{1,i}, \chi_{2,i}, \ldots, \chi_{c,i}), \Xi(\chi_{1,i+\boldsymbol{\tau_1}}, \chi_{2,i+\boldsymbol{\tau_2}}, \ldots, \chi_{c,i+\boldsymbol{\tau_c}}), \\ &\ldots, \Xi(\chi_{1,i+(\mathbf{M}-1)\boldsymbol{\tau_1}}, \chi_{2,i+(\mathbf{M}-1)\boldsymbol{\tau_2}}, \ldots, \chi_{c,i+(\mathbf{M}-1)\boldsymbol{\tau_c}})] \end{aligned} \tag{2}$$

where Ξ indicates the median value of the samples, and $\mathbf{M} = max([m_1, m_2, \ldots, m_c])$ is the dimension of the c-variate phase space. The maximum value is chosen to avoid an underestimation of the attractor dimension.

Second, the Chebyshev distance d between multivariate vectors $Z_{\mathbf{M}}$, i.e., the maximum absolute difference of their scalar components, is calculated. A fuzzy membership function $\Gamma(d, r)$ is then calculated as follows [26]:

$$\Gamma(d, r) = e^{\frac{-d^{f_c}}{r}} \tag{3}$$

with f_c indicating the so-called fuzzy power. For our analyses we used the value $f_c = 2$ [26]. As a refined approach, in order to prevent the influence of the reduced variance of the coarse-grained series at higher scales, the threshold r varies according to the scale factor β:

$$r = 0.15 \times (std(\Psi_1^{(\beta)}) + std(\Psi_2^{(\beta)}) + \cdots + std(\Psi_c^{(\beta)})) \tag{4}$$

where $\Psi_k^{(\beta)}$, with $k = 1, 2, \ldots, c$, are the scaled multivariate series for each scale factor β, after the coarse-graining procedure. The multiplying factor 0.15 is taken from the literature [24–26,45].

By defining a quantity $\Phi^{\mathbf{M}}(r)$ as the average membership grade:

$$\Phi^{\mathbf{M}}(r) = \frac{1}{(N-\nu)} \sum_{i=1}^{N-\nu} \frac{\sum_{j=1, i\neq j}^{N-\nu} e^{\left(\frac{-(d[Z_{\mathbf{M}}(i), Z_{\mathbf{M}}(j)])^{f_c}}{r}\right)}}{N-\nu-1} \tag{5}$$

with $\nu = \mathbf{T} \times \mathbf{M}$ (where $\mathbf{T} = max([\tau_1, \tau_2, \ldots, \tau_c])$), it is possible to finally compute the MCI multivariate metrics as follows:

$$\Lambda_{\mathrm{MCI}}(\mathbf{Y}, \beta, \mathbf{T}, \mathbf{M}, \mathrm{r}) = -ln\left(\frac{\Phi^{(\mathbf{M}+1)}(r)}{\Phi^{\mathbf{M}}(r)}\right) \tag{6}$$

From the multiscale trends of Λ_{MCI}, we extracted two MCI values quantifying the area under the curve of the entropy levels as a function of the scale factor β into two different ranges [46–48]:

- MCI_{short}: area under the curve of Λ_{MCI} considering the range $\beta \in [1, 5]$ of fast multi-organ oscillations;
- MCI_{long}: area under the curve of Λ_{MCI} considering the range $\beta \in [6, 20]$ of slow multi-organ oscillations.

2.2. RCmvMFE at a glance

Performance of the proposed MCI is compared with the state of the art metrics concerning multivariate complexity. To this aim, we refer to the Refined Composite Multivariate Multiscale Fuzzy Entropy (RCmvMFE) [26], which uses the technique described in Section 2.1 to check the similarity between embedded vectors, based on the fuzzy function $\Gamma(d, r)$. Unlike MCI, the coarse graining step follows the refined composite procedure [41]. β coarse grained multivariate time series are generated for each value of scale factor: $z_{\alpha}^{(\beta)} = \left\{x_{\alpha,n,i}^{\beta}\right\}$, with $1 \leq \alpha \leq \beta$, as follows:

$$ {}^{\mu}\chi_{\alpha,n,i}^{(\beta)} = \frac{1}{\beta} \sum_{b=(i-1)\beta+1}^{i\beta+\alpha-1} y_{n,b} \tag{7} $$

$$ where \quad 1 \leq i \leq \left\lfloor \frac{L}{\beta} \right\rfloor = N, \quad 1 \leq k \leq c \tag{8} $$

Then, the multivariate embedded vectors $X(m)$ of the phase space are constructed concatenating the embedded vectors of all c series and are defined as:

$$ X(m) = \left[\chi_{1,i}, \chi_{1,i+\tau_1}, \ldots, \chi_{1,i+(m_1-1)\tau_1}, \chi_{2,i}, \chi_{2,i+\tau_2}, \ldots, \chi_{2,i+(m_2-1)\tau_2}, \ldots, \chi_{c,i}, \chi_{c,i+\tau_c}, \ldots, \chi_{c,i+(m_c-1)\tau_c}\right] \tag{9} $$

When the dimensionality of the multivariate delay vector is extended from m to $(m+1)$, c different embedded vectors are obtained, adding a sample to one variable h while the other $c-1$ variables are unchanged. The global quantity $\Phi^{m+1}(r)$ is computed as the average of the values of $\Phi^{m_h+1}(r)$, with $1 \leq h \leq c$.

In order to compare the results obtained by applying RCmvMFE with the proposed MCI_{short} and MCI_{long} indexes, we used the same τ and m values (calculated as described in Section 2.1) for the corresponding time series in the computation of both algorithms. Also for RCmvMFE, we computed two complexity indexes (ci), i.e., CI_{short} and CI_{long}, from the trends of RCmvMFE as a function of β. We considered the range $\beta \in [1, 5]$ for $RCmvMFE_{CI_{short}}$ and $\beta \in [6, 20]$ for $RCmvMFE_{CI_{long}}$.

2.3. Experimental data

MCI and RCmvMFE indices are estimated from experimental data including bivariate and trivariate synthetic and real physiological processes. Details follow below.

2.3.1. Synthetic data

White gaussian noise and 1/f noise

We first test the MCI method on simulated systems defined through white gaussian noise (WGN) and 1/f noise, as reported in [5,24,26]. We generated 50 realizations of a system comprising three correlated WGN series and 50 realizations of a system comprising three correlated 1/f noise series, both with a correlation coefficient $\rho = 0.75$. We started from a 3-channel matrix H comprising three uncorrelated signals and computed the corresponding upper triangular matrix L from the Cholesky decomposition of a defined correlation matrix R to set the correlation by multiplying H by L [26]. We then compared MCI values estimated from the WGN and 1/f systems, expecting different multiscale trends, consistently with the fact that 1/f noise shows complex structures across multiple time scales.

In the second test, we compare MCI values estimated on (i) 50 realizations generated from a system comprising two correlated signals (with correlation $\rho = 0.75$) and one uncorrelated signal, and (ii) 50 realizations generated from a system comprising a 3-channel fully correlated series ($\rho = 0.75$). This test was repeated twice selectively considering series of WGN and 1/f noise. Each series comprised 4000 samples.

Moreover, we derived MCI estimates from synthetic series generated from the Hénon map and Rössler attractor, and we compared our results with RCmvMFE estimates. The Hénon map is a bivariate nonlinear dynamical system, whereas the Rössler attractor is a nonlinear trivariate system, and both exhibit complex behaviour as per the specific parameters set in their canonical equations. We use the same τ and m values to compare MIC and RCmvMFE performances, as described in Section 2.1. Inspired by our previous endeavours [36,49], the canonical equations were slightly modified to include a stochastic term allowing for the study of MCI and RCmvMFE estimates as a function of the noise variance.

Bivariate Hénon Map

A bivariate stochastic Hénon map was implemented according to the following iterative equation [36]:

$$ \begin{cases} x_{n+1} = 1 - ax_n^2 + y_n + k\epsilon(t) \\ y_{n+1} = bx_n + k\epsilon(t) \end{cases} \tag{10} $$

where $\epsilon(t)$ indicates independent identically distributed Gaussian random variables with zero mean and unit variance. A total of 200 realizations of 10^5 samples were generated for each of the 28 different values of k in the range $k \in [3 \times 10^{-3}, 3 \times 10^{-2}]$, with a step size of 10^{-3}.

Table 1
Subjects information for the postural change dataset.

Subjects ID	Gender	Age (years)	Height (cm)	Weight (kg)
12726	M	28	170	64
12734	M	30	165	64
12744	M	28	180	100
12754	F	26	160	61
12755	M	32	192	83
12814	F	27	165	56
12815	F	22	185	73
12819	F	28	155	55
12821	F	32	173	77
13960	M	34	183	83
		28.7 ± 1.2	172.8 ± 4.0	70.6 ± 4.5

These data were generated for $a = 1.00$ and $a = 1.09$ (100 realizations for each group), while fixing $b = 0.3$. In fact, the transition between the non-chaotic and chaotic regime for the Henón map in a purely deterministic domain is marked by the threshold value $a = 1.07$.

For each realization multivariate entropy values were extracted using 20 values of scale factor β, and two ranges of β were used to compute the CI, as described in 2.1.

Trivariate Rössler Attractor

A trivariate stochastic Rössler attractor was implemented as per the following differential equations [36,49]:

$$\begin{cases} \dfrac{dx}{dt} = -y - z + k\epsilon(t) \\ \dfrac{dy}{dt} = x + ay + k\epsilon(t) \\ \dfrac{dz}{dt} = b + z(x - c) + k\epsilon(t) \end{cases} \tag{11}$$

whose behaviour depends on the parameters set $\{a, b, c\}$. A total of 50 realizations were generated using the fifth-order Runge–Kutta method for each of the 28 different values of k in the range $k \in [3 \times 10^{-3}, 3 \times 10^{-2}]$, with a step size of 10^{-3}.

These data were generated for $a = 0.20$, as well as for $a = 0.45$, while fixing $b = 2$ and $c = 4$. In fact, the transition between the non-chaotic and chaotic regime for the Rössler attractor in a purely deterministic domain corresponds to the $a = 0.432$.

For each realization, we generated 10^5 data points using a time-step size of 0.02. The range used for the scale factor β was [1,21], CI_{short} was computed in the range [1,5] and CI_{long} in the range [6,21].

2.3.2. Physiological data

We evaluated the MCI vs. RCmvMFE performance as related to real multi-organ interplay in two cardiovascular physiology studies including time series from heartbeat and blood pressure dynamics.

Particularly, we investigated bivariate cardiovascular dynamics in healthy subjects undergoing three different postural changes [38,50], as well as trivariate cardiovascular dynamics in healthy young adults and elderly subjects while watching the movie "Fantasia" (Disney, 1940) [40]. Both datasets are publicly available [39].

Starting from ECG and blood pressure series, a bivariate analysis considering HRV and DITV was performed on the postural changes dataset, whereas a trivariate analysis considering HRV, STIV, and DTIV series was performed on the "Fantasia" dataset.

We used the automatic algorithm developed by Pan–Tompkins to automatically identify the RR series from the ECG [51]. Artefacts and ectopic beats were corrected through the use of Kubios HRV software [52].

Blood pressure signals were pre-processed through a Butterworth-approximated band-pass filter with 0.05–40 Hz band. Once local maxima and minima were identified, STIV series were obtained as time intervals between consecutive systolic beats, whereas DTIV series were obtained from time intervals between consecutive diastolic beats. A shape-preserving piecewise cubic interpolation at the standard rate of 4 Hz was applied to all series.

Multivariate entropy indices were computed considering the first 5 coarse-grained series of the biosignals recorded during postural changes, and the first 20 coarse-grained series of the biosignals recorded during "Fantasia" watching.

Postural Changes Dataset

Extensive details on this experimental protocol are reported in [38,50]. Briefly, ten healthy volunteers (five females) with no sign of cardiovascular diseases were recruited in the study. Table 1 reports subjects' information regarding gender, age, weight, and height.

Each subjects underwent the following postural changes in a randomized order among subjects, being separated by five minutes of resting state in a supine position:

- two stand-ups;
- two rapid head-up tilt (75° over 2 s);
- two slow head-up tilt (75° over 50 s).

After the postural change, each subject was asked to remain in a upright position for three minutes.

The experiment protocol was approved by the Advisory Board of the MIT-MGH General Clinical Research Center and the MIT's Committee on the Use of Humans as Experimental Subjects. Throughout all experiment, continuous ECG signal and blood pressure were non-invasively acquired by means of a standard ECG monitor system (BIOPAC MP System) and a non-invasive blood pressure monitoring device (2300 FINAPRES BP monitor), respectively. ECG signals were acquired following the lead II configuration, while blood pressure was recorded at the second phalanx of the left middle finger.

Fantasia Dataset

Extensive details on this experimental protocol are reported in [40]. Briefly, a total of 20 young (10 females; age range: 21–34 years) and 20 elderly (10 females; age range: 68–85 years) healthy subjects underwent 120 min of continuous monitoring of autonomic signs in a supine position while the movie "Fantasia" (Disney movie, 1940) was projected to maintain the subject's wakefulness. In 10 subjects per group, ECG series were acquired along with uncalibrated continuous non-invasive blood pressure signals, all sampled at 250 Hz. Each heartbeat was annotated using an automated arrhythmia detection algorithm, and verified through visual inspection.

The proposed MCI was estimated considering a trivariate process comprising HRV series derived from the ECG, diastolic and systolic blood pressure variability (DTIV and STIV). Pre-processing steps were the same as for the postural changes dataset (see previous paragraph).

2.4. Statistical analysis

We used non-parametric tests given the non-gaussian distribution of samples, as demonstrated by the application of Shapiro–Wilk test. According to the nature of data samples, we chose to use Mann–Whitney test for unpaired samples, and Wilcoxon test for paired samples. Mann–Whitney non-parametric test was used to compare the MCI values obtained using WGN and 1/f noise as input.

For both Henón and Rosslër systems, Mann–Whitney non-parametric tests were used to compare CI_{short} and CI_{long} values between the two groups of realizations related to the different complexity regimes. Such a statistical testing was iterated for each of the 28 realizations obtained at different noise variance.

Concerning the postural changes dataset, Wilcoxon non-parametric tests for paired data were employed to compare both CI_{short} and CI_{long} between supine resting state vs. upright (i.e., resting vs. stand-up; resting vs. rapid-tilt; and resting vs. slow-tilt).

Concerning the Fantasia dataset, Mann–Whitney non-parametric tests were employed to compare both CI_{short} and CI_{long} between young adults and elderly subjects.

3. Results

3.1. Synthetic series

3.1.1. White Gaussian noise and 1/f noise trivariate systems

Fig. 1 shows MCI trends and statistics in discerning between a 3-channel system comprising fully correlated WGN and a 3-channel system with fully correlated 1/f noise ($\rho = 0.75$). While MCI trends tend to remain constant along the scales for 1/f noise, a monotonic decrease seems to be associated with WGN. Quantitatively, we found that Λ_{MCI} values were significantly different for the two systems ($p < 0.05$ for all the scales, Λ_{MCI} higher in 1/f noise than WGN for $\beta \in [2, 20]$), and both MCI_{short} and MCI_{long} were significantly higher for 1/f noise than WGN, with $p < 10^{-9}$ and $p < 10-17$ respectively. These outcomes confirm that MCI can be considered as a measure of complexity, and not a measure of series irregularity, as well as confirm the hypothesis that a greater complexity level is associated with 1/f noise at scales higher than 2.

On the other hand, Fig. 2 shows MCI trends and statistics in discerning between a 3-channel system comprising fully correlated signals (S1) and a 3-channel system with 2 correlated signals ($\rho = 0.75$) and one uncorrelated signal (S2). This procedure was iterated twice to implement WGN and 1/f noise. We found significant p-values related to Λ_{MCI} for all the scales, and to MCI at short and long scales. In all the cases, highest values of MCI and Λ_{MCI} were found for a fully correlated system.

3.1.2. Henón map

For the stochastic Henón map, Fig. 3 show boxplots statistics for CI_{short} and CI_{long}, as a function of k in the range $[3 \times 10^{-3}, 3 \times 10^{-2}]$, computed from MCI and RCmvMFE.

Table 2 reports the results from the Mann–Whitney tests on *MCI* and CI_{short} and CI_{long} from RCmvMFE. Computing MCI_{short}, the two state of Henón system (non-chaotic vs. chaotic) were always found to be statistically different, with a p-value less than 10^{-33} for all the levels of noise. As we expected, the chaotic-like behaviour of the synthetic system was identified by higher values of MCI in comparison with the non-chaotic dynamics. On the other side, CI_{short} values

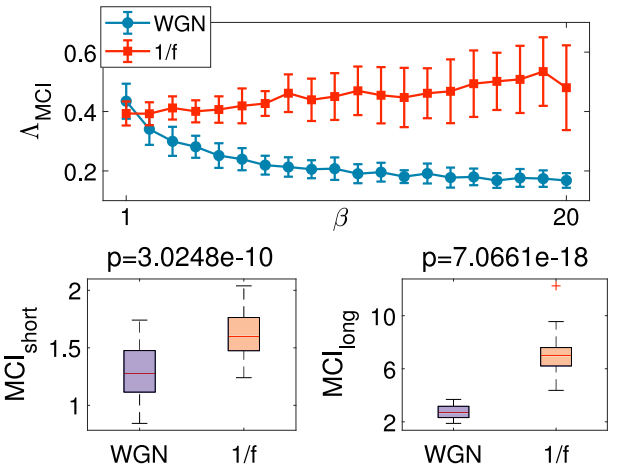

Fig. 1. Trends of Λ_{MCI} as a function of β for 50 realizations of 3-channel correlated WGN signals and 50 realizations of 3-channel correlated 1/f signals (on the top). On the bottom the boxplots of MCI_{short} (on the left) and MCI_{long} (one the right) are reported, together with the related p-values. WGN and 1/f results are shown in blue and red, respectively.

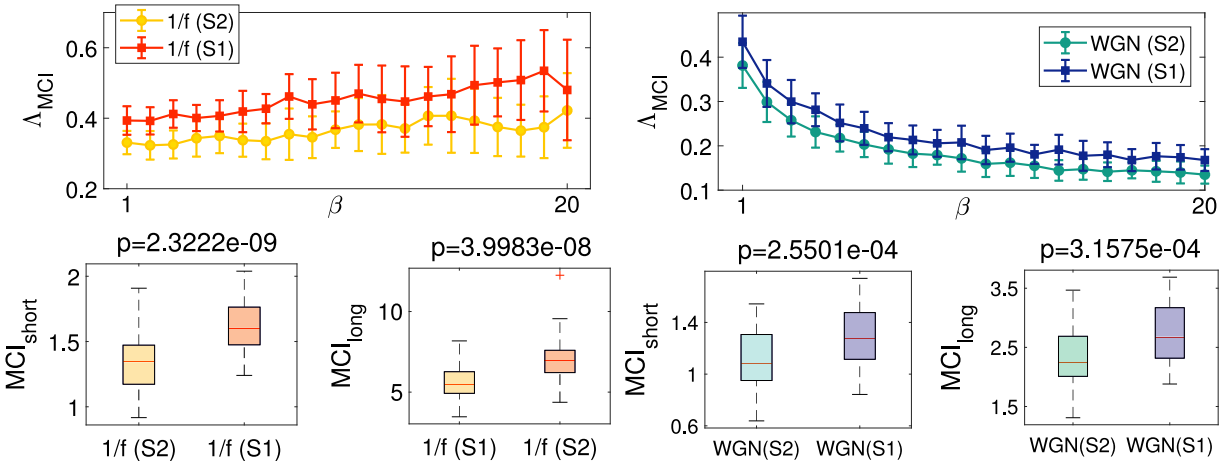

Fig. 2. On the left: trends of Λ_{MCI} as a function of β for 50 realizations of 3-channel correlated 1/f signals (1/f (S1), red) and 50 realizations of 2-channel correlated 1/f signals and one uncorrelated 1/f signal (1/f (S2), yellow). On the right: trends of Λ_{MCI} as a function of β for 50 realizations of 3-channel correlated WGN signals (WGN (S1), dark blue) and 50 realizations of 2-channel correlated WGN signals and one uncorrelated WGN signal (WGN (S2), light blue). On the bottom of each figure, the boxplots of MCI_{short} (on the left) and MCI_{long} (one the right) are reported, together with the related p-values.

computed on RCmvMFE trends discriminated the two stated as significantly different, but the values referred to a $= 1.00$ were the highest.

Concerning the long scale range, MCI_{long} were higher in the chaotic state than the non-chaotic one ($p < 10^{-14}$), except for the range $k \in [0.012, 0.017]$. As regards RCmvMFE, the results of statistical tests gave significant p-values, but for $k > 0.01$ CI_{long} was higher in the case $a = 1.00$.

3.1.3. Rössler attractor

Fig. 4 shows the results from MCI and RCmvMFE applied to Rössler attractor series. Results from Mann–Whitney statistical tests for both MCI and RCmvMFE are shown in Table 3.

The CIs values from the proposed MCI were always statistically different between the two system states (at $a = 0.20$ and $a = 0.45$), with the chaotic behaviour associated with higher CIs with respect to the non-chaotic one. The only exception is represented by MCI_{long} for k $= 0.011$ which gave non-significant results.

Concerning RCmvMFE, results show significant p-values, although higher complexity was associated with a non-chaotic behaviour at $a = 0.20$ for all the values of k at short scales, and for $k \leq 0.015$ at long scales.

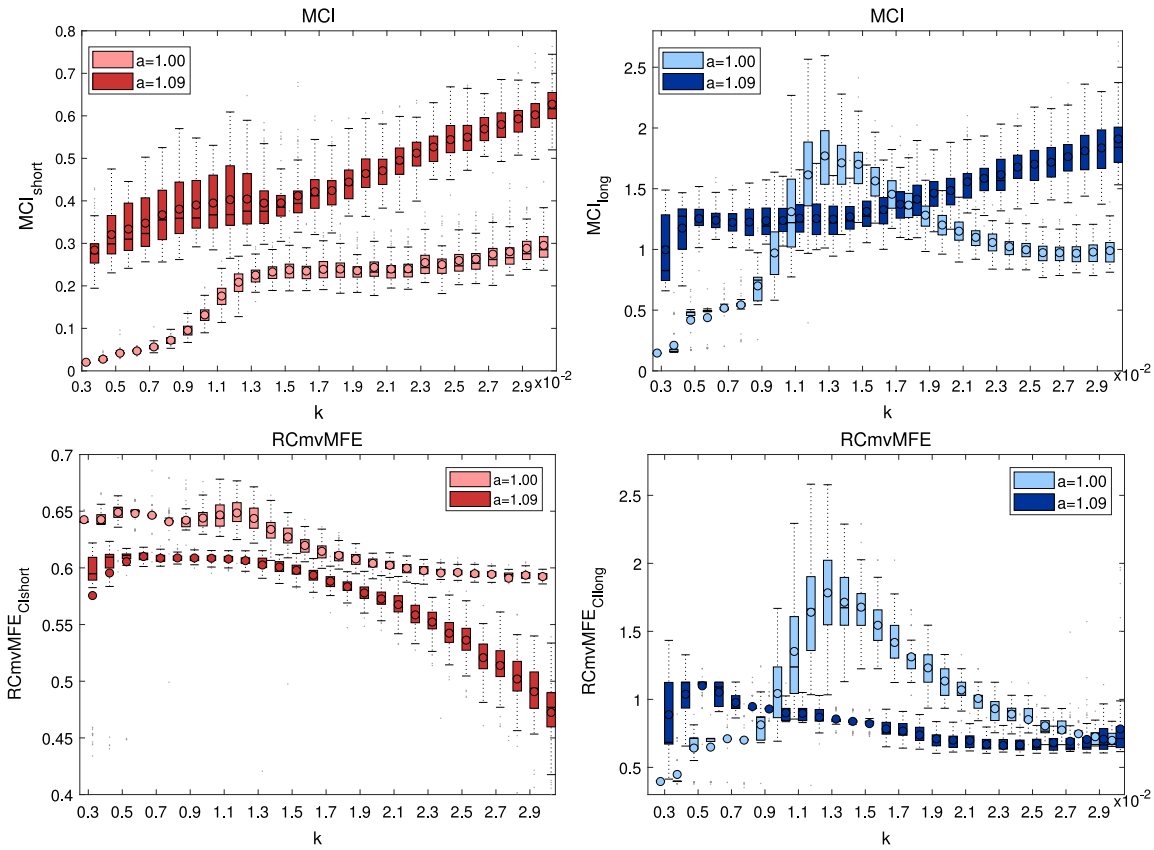

Fig. 3. Boxplots of CI_{short} and CI_{long} values from the proposed MCI (on the top) and RCmvMFE (on the bottom). CI values were computed using the two series of the Henón map system.

Table 2
Results of Mann–Whitney statistical test between chaotic (C, a = 1.09) and non-chaotic (NC, a = 1.00) realizations of the Hénon map for each value of k. The statistical tests were computed on the CI_{short} and CI_{long} indexes.

	CI_{short}	CI_{long}
MCI	$CI_{short}(NC) < CI_{short}(C)$ $p < 10^{-33}$ $\forall$ k	$CI_{long}(NC) < CI_{long}(C)$ $p < 10^{-17}$ per $k \leq 0.01$
		n.s. per k = 0.011
		$CI_{long}(NC) > CI_{long}(C)$ $p < 10^{-3}$ per $0.012 \leq k \leq 0.0.17$
		n.s. per k = 0.018
		$CI_{long}(NC) < CI_{long}(C)$ $p < 10^{-14}$ per $k > 0.018$
RCmvMFE	$CI_{short}(NC) > CI_{short}(C)$ $p < 10^{-30}$ $\forall$ k	$CI_{long}(NC) < CI_{long}(C)$ $p < 10^{-15}$ per $k < 0.01$
		$CI_{long}(NC) > CI_{long}(C)$ $p < 10^{-3}$ per $0.01 \leq k < 0.029$
		n.s. per k = 0.03

3.2. Experimental data

3.2.1. Tilt-table experiment

On the postural change dataset, we considered MCI and RCmvMFE estimates computed from the first two minutes of stand-up, rapid-tilt, and slow-tilt after the transition phase as compared with multivariate complexity estimated from the last two minutes of the corresponding preceding resting-state. Given the duration of the series, we considered only the CI_{short} referred to the first two scales for the analysis of these signals.

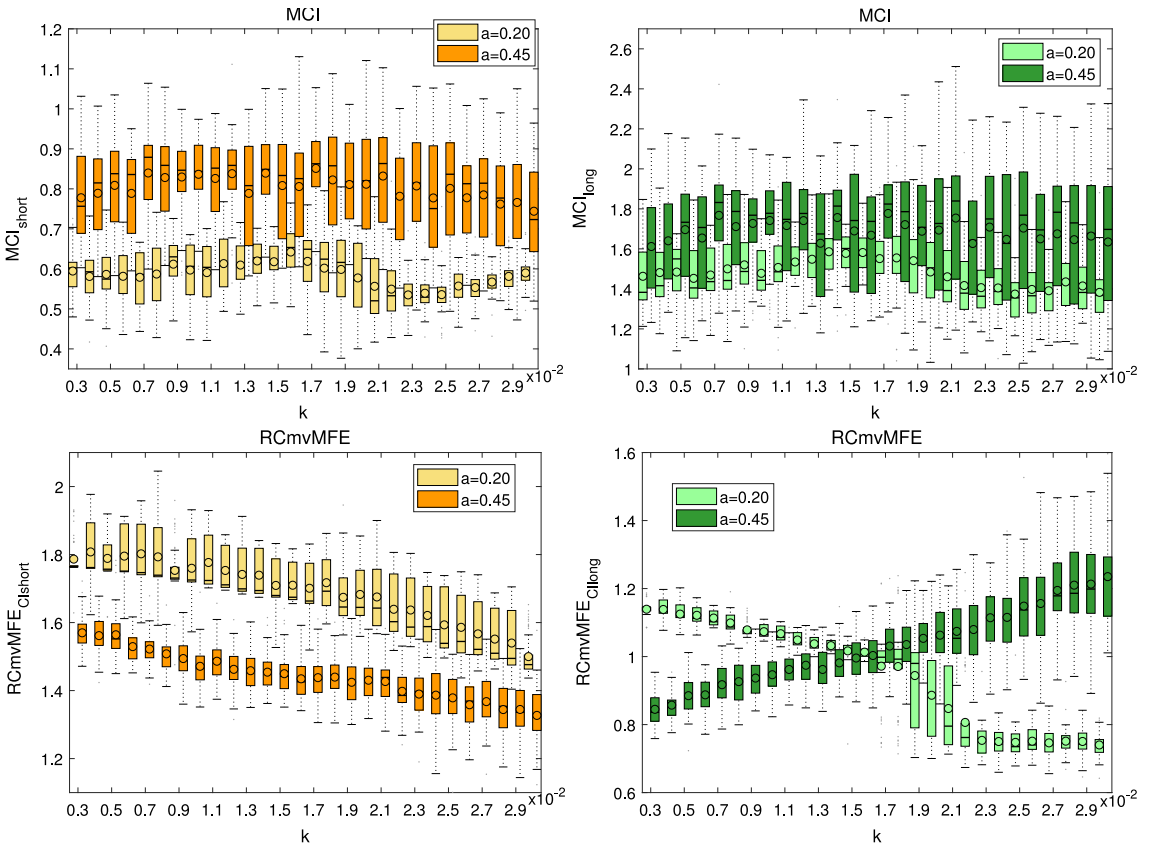

Fig. 4. Boxplots of CI_{short} and CI_{long} values from the proposed MCI (on the top) and RCmvMFE (on the bottom). CI values were computed from the three series of the Rössler system.

Table 3
Results of Mann–Whitney statistical test between chaotic (C, a = 0.45) and non-chaotic (NC, a = 0.20) realizations of the Rössler system for each value of k. Statistical tests were computed on the CI_{short} and CI_{long} indexes.

	CI_{short}	CI_{long}
MCI	$CI_{short}(NC) < CI_{short}(C)$ $p < 10^{-9}$ $\forall$ k	$CI_{long}(NC) < CI_{long}(C)$ $p < 10^{-3}$ per $k \leq 0.01$
		n.s. per k = 0.011
		$CI_{long}(NC) < CI_{long}(C)$ $p < 0.03$ per $0.012 \leq k \leq 0.03$
RCmvMFE	$CI_{short}(NC) > CI_{short}(C)$ $p < 10^{-14}$ $\forall$ k	$CI_{long}(NC) > CI_{long}(C)$ $p < 10^{-2}$ per $k \leq 0.015$
		n.s. per k = 0.016
		$CI_{long}(NC) < CI_{long}(C)$ $p < 0.03$ per le $k > 0.016$

Figs. 5 and 6 show the results related to *MCI* and RCmvMFE estimates, respectively.

Note that, for each postural change in Fig. 5, the median values of MCI were higher during rest condition than during tilt and stand-up. The p-values related to Wilcoxon statistical test were always significant ($p < 0.05$).

Concerning the results from the RCmvMFE method, slow-tilt resulted to be associated with statistically lower CI_{short}, when compared to the preceding resting state (p = 0.0438). However, we did find statistically significant differences between supine resting state and rapid tilt and between supine resting state and stand-up, as shown in Fig. 6.

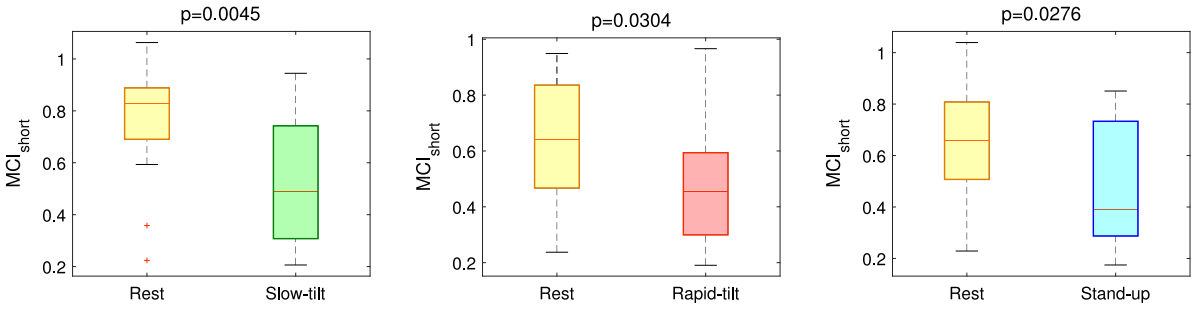

Fig. 5. MCI boxplots statistics for the postural changes dataset. Estimates were computed for slow-tilt, rapid-tilt, and stand-up sessions and compared with the preceding resting state session. Corresponding p-values from Wilcoxon non-parametric tests are reported for each comparison.

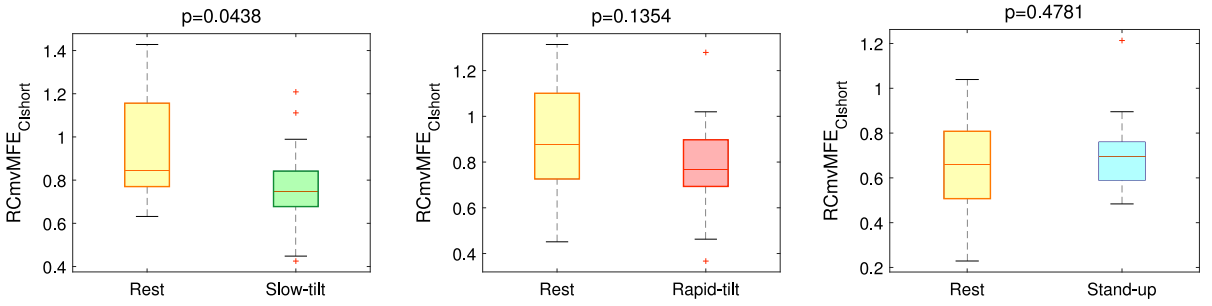

Fig. 6. RCmvMFE boxplots statistics for the postural changes dataset. Estimates were computed for slow-tilt, rapid-tilt, and stand-up sessions and compared with the preceding resting state session. Corresponding p-values from Wilcoxon non-parametric tests are reported for each comparison.

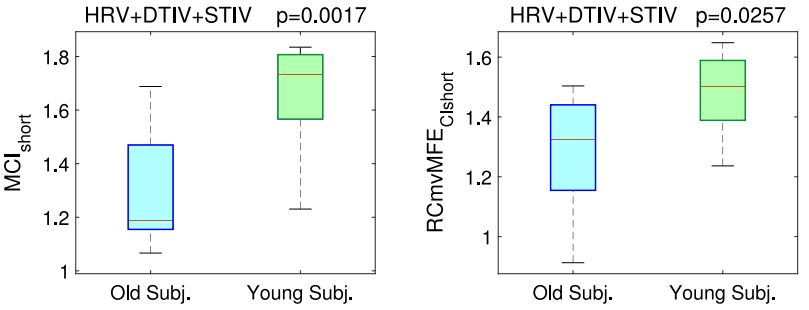

Fig. 7. Boxplots of the results obtained computing MCI_{short} on Fantasia dataset. The trivariate case is reported on the left, using HRV, DTIV, and STIV. The other two plots are referred to bivariate cases: using HRV and STIV (in the middle) and using HRV and DTIV (on the right).

3.2.2. Fantasia database

Fig. 7 shows trends from the proposed MCI vs. RCmvMFE in discerning young from old subjects of the Fantasia experiment using HRV, DTIV, and STIV, at short scales. Both methods associated higher autonomic complexity to young subjects than elderly, with $p = 0.0017$ for MCI and $p = 0.0257$ for RCmvMFE.

In Fig. 8 the result concerning the long scale range are reported. Even if young people showed higher complexity than old subjects using both algorithms, we found a significant *p*-value only in MCI case ($p = 0.0312$).

4. Discussion

This study introduces the MCI as a novel signal processing tool for the complexity assessment of multi-organ interacting systems, while accounting for their multivariate-multiscale physiological dynamics. Particularly, MCI embeds new metrics from a multivariate phase space reconstruction, which can be useful for describing complex systems, such as the ANS, comprising multiple outputs with different temporal scales.

In the proposed MCI approach, each time series of the multivariate system is associated with a specific time delay (τ) and a specific τ-related embedding dimension (m) to avoid the "curse of dimensionality" issue [13,29,30].

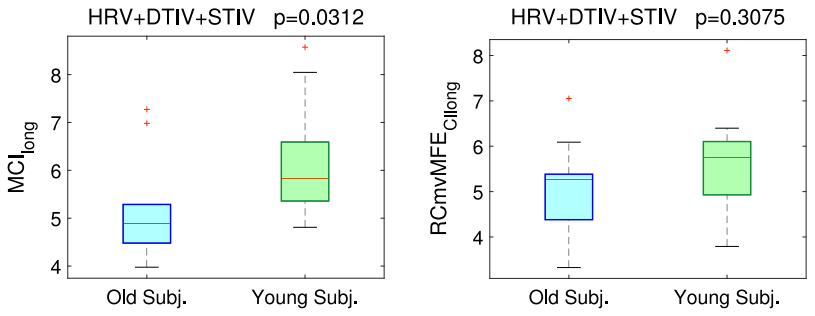

Fig. 8. Boxplots of the results obtained computing MCI_{long} on Fantasia dataset. The trivariate case is reported on the left, using HRV, DTIV, and STIV. The other two plots are referred to bivariate cases: using HRV and STIV (in the middle) and using HRV and DTIV (on the right).

State of the art metrics for multivariate complexity are best suitable for long-term series. Also, such metrics computation might be time consuming, therefore limiting prospective mobile health applications. The proposed MCI approach overcomes this limitation by also considering the median values of the multivariate phase-space coordinates, such that our embedding approach has a low computational cost while accounting for a non-parametric calculation of the system dynamics central tendency.

Moreover, the implementation of a fuzzy rule (on the basis of an exponential function) to quantify the match between embedded vectors reduces possible biases from the free parameters choice. The thresholding procedure is also redefined for each scaled series according to the series standard deviation, thus avoiding biased estimations due to the reduced scale-dependent variance.

We tested the proposed MCI in synthetic and experimental datasets considering bivariate and trivariate systems, and compared the performance with a previously defined fuzzy entropy algorithm, the RCmvMFE [26].

Results clearly point out that the proposed MCI metrics is able to discern between different levels of complexity and coupling in stationary multivariate systems, as demonstrated through simulation of WGN and 1/f noise processes. Specifically, a MCI increase was associated with an increase in a sub-system coupling, both at shorter and higher scales.

Moreover, considering bivariate Hénon maps and trivariate Rössler attractors, the proposed MCI was able to discern between two states associated with two different levels of interaction, for both short- and long-scales (see Tables 2 and 3 and Figs. 3 and 4). An interesting trend of Λ_{MCI} as a function of k was found for the Rössler attractor at long-scales. In fact, a stochastic resonance-like behaviour induced by noise was recognized.

On real data, the proposed MCI shows improved performance than RCmvMFE considering physiological complexity modulation due to sympatho-vagal changes, also from a baroreflex modulation (postural changes), and ageing. Particularly, considering bivariate HRV and DTIV series as input, we found a significant decrease in multivariate complexity as estimated through MCI following each postural change, with respect to the previous supine resting state. This is in agreement with previous investigations on univariate cardiovascular complexity [15,35,36,53], as well as previous studies on causal coupling between HRV and blood pressure variability series during postural changes [54,55]. This also allows us to conclude that the complexity of the multivariate interplay between the cardiovascular system and the ANS decreases following a postural changes (i.e., a significant sympatho-vagal change). Considering the series under study as stationary, we may conclude that such a MCI decrease implies a reduction of coupling between the cardiovascular system subcomponents, which has already been reported in [56]. Note that RCmvMFE showed a significant difference in the case of slow-tilt exclusively (see Fig. 6).

On the ageing dataset, the proposed MCI was always associated with a significant p-value in discerning young vs. elderly subjects using trivariate dynamics from HRV, DTIV and STIV series. Note also that the multivariate cardiovascular complexity was lower in the elderly than in the young, which is consistent with previous findings on univariate cardiovascular complexity [5]. Conversely, RCmvMFE did not provide significant results at long-scales.

A possible explanation for the improved MCI performance with respect to RCmvMFE could be the construction of multivariate embedded vectors. In fact, while RCmvMFE vectors dimension in the multivariate phase space reconstruction is estimated through the sum of the dimensions associated with each series, therefore possibly resulting in an overestimation of the actual phase space dimension [24–26], the proposed MCI employs a non-parametric measure of central tendency, possibly balancing between the contribution of multiple dynamics occurring at a different time scale. Distinctive features of the proposed MCI are also the coarse-graining procedure computed through non-overlapping time vectors, and the step-by-step update of the radius threshold according to the standard deviation of each scaled series. On the other hand, RCmvMFE implements coarse-graining procedures with overlapping vectors in time, which might bias the actual entropy estimation.

Our findings suggest that the MCI approach improves on the state of the art on multivariate complexity assessment, especially at shorter scales (from 1 to 5). In fact, a significant p-value was found from the first scale in analysing synthetic stationary systems with different levels of subsystem coupling (see Section 2.3.1 and Fig. 2). On the other hand, higher

MCI values were found in 1/f noise systems than in WGN ones in the range $\beta \in [2, 20]$ (see Fig. 1). The MCI analysis of Hénon and Rössler systems provided meaningful results at short-scales as well. For both systems, while $RCmvMFE_{CIshort}$ decreases in chaotic-like conditions, MCI_{short} increased for each level of additive noise.

We then exploited these calculations on short-time physiological signals, where only short-scales could be analysed. On the postural changes protocol, MCI_{short} was lower during each upright phase than resting state, whereas a significant decrease in $RCmvMFE_{CIshort}$ was found during the slow-tilt phase only. We believe that the significance of results using the MCI approach at short-scales is one of the strengths of this method, allowing the study of multivariate short-time series.

In conclusion, the proposed MCI can be considered as a viable signal processing tool for the complexity analysis of multichannel physiological recordings, especially related to multivariate ANS dynamics on cardiovascular control.

Future endeavours will be directed to further applications of multivariate physiological systems, especially focusing on brain–brain and brain–heart interplay, paving also the way towards the study of complex multimodal dynamics (i.e., from imaging, electrophysiology, biomarkers, etc.).

Appendix

The Matlab code for MCI estimation is publicly available online at https://github.com/NardelliM/MCI.

References

[1] A.L. Goldberger, C.-K. Peng, L.A. Lipsitz, What is physiologic complexity and how does it change with aging and disease?, Neurobiol. Aging 23 (1) (2002) 23–26.
[2] M. Mitchell, Complexity: A Guided Tour, Oxford University Press, 2009.
[3] R. Barbieri, E.P. Scilingo, G. Valenza, Complexity and Nonlinearity in Cardiovascular Signals, Springer, 2017.
[4] A. Voss, S. Schulz, R. Schroeder, M. Baumert, P. Caminal, Methods derived from nonlinear dynamics for analysing heart rate variability, Philos. Trans. R. Soci. Lond. A 367 (1887) (2009) 277–296.
[5] M. Costa, A.L. Goldberger, C.-K. Peng, Multiscale entropy analysis of complex physiologic time series, Phys. Rev. Lett. 89 (6) (2002) 068102.
[6] V.Z. Marmarelis, Nonlinear Dynamic Modeling of Physiological Systems, Vol. 10, John Wiley & Sons, 2004.
[7] R. Sassi, S. Cerutti, F. Lombardi, M. Malik, H.V. Huikuri, C.-K. Peng, G. Schmidt, Y. Yamamoto, D. Reviewers:, B. Gorenek, et al., Advances in heart rate variability signal analysis: joint position statement by the e-Cardiology ESC working group and the european heart rhythm association co-endorsed by the asia pacific heart rhythm society, Ep Europace 17 (9) (2015) 1341–1353.
[8] K. Sunagawa, T. Kawada, T. Nakahara, Dynamic nonlinear vago-sympathetic interaction in regulating heart rate, Heart Vessels 13 (4) (1998) 157–174.
[9] F. Beissner, K. Meissner, K.-J. Bär, V. Napadow, The autonomic brain: an activation likelihood estimation meta-analysis for central processing of autonomic function, J. Neurosci. 33 (25) (2013) 10503–10511.
[10] H. Kantz, J. Kurths, G. Mayer-Kress, Nonlinear Analysis of Physiological Data, Springer Science & Business Media, 2012.
[11] D.A. Drachman, Aging of the brain, entropy, and alzheimer disease, Neurology 67 (8) (2006) 1340–1352.
[12] S.M. Pincus, Approximate entropy as a measure of system complexity., Proc. Natl. Acad. Sci. 88 (6) (1991) 2297–2301.
[13] J.S. Richman, J. Moorman, Physiological time-series analysis using approximate entropy and sample entropy, Amer. J. Physiol.-Heart Circ. Physiol. 278 (6) (2000) H2039–H2049.
[14] G. Valenza, M. Nardelli, A. Lanata, C. Gentili, G. Bertschy, M. Kosel, E.P. Scilingo, Predicting mood changes in bipolar disorder through heartbeat nonlinear dynamics, IEEE J. Biomed. Health Inform. 20 (4) (2016) 1034–1043.
[15] A. Porta, T. Gnecchi-Ruscone, E. Tobaldini, S. Guzzetti, R. Furlan, N. Montano, Progressive decrease of heart period variability entropy-based complexity during graded head-up tilt, J. Appl. Physiol. 103 (4) (2007) 1143–1149.
[16] L.A. Lipsitz, A.L. Goldberger, et al., Loss of complexity and aging, JAMA 267 (13) (1992) 1806–1809.
[17] D.T. Schmitt, P.C. Ivanov, Fractal scale-invariant and nonlinear properties of cardiac dynamics remain stable with advanced age: a new mechanistic picture of cardiac control in healthy elderly, Amer. J. Physiol.-Regul. Integr. Comp. Physiol. 293 (5) (2007) R1923–R1937.
[18] D.T. Schmitt, P.K. Stein, P.C. Ivanov, Stratification pattern of static and scale-invariant dynamic measures of heartbeat fluctuations across sleep stages in young and elderly, IEEE Trans. Biomed. Eng. 56 (5) (2009) 1564–1573.
[19] J.F. Valencia, A. Porta, M. Vallverdu, F. Claria, R. Baranowski, E. Orlowska-Baranowska, P. Caminal, Refined multiscale entropy: Application to 24-h holter recordings of heart period variability in healthy and aortic stenosis subjects, IEEE Trans. Biomed. Eng. 56 (9) (2009) 2202–2213.
[20] M. Costa, A.L. Goldberger, C.-K. Peng, Multiscale entropy analysis of biological signals, Phys. Rev. E 71 (2) (2005) 021906.
[21] L.E.V. Silva, B.C.T. Cabella, U.P. da Costa Neves, L.O.M. Junior, Multiscale entropy-based methods for heart rate variability complexity analysis, Physica A 422 (2015) 143–152.
[22] J. Hu, J. Gao, W.-w. Tung, Y. Cao, Multiscale analysis of heart rate variability: a comparison of different complexity measures, Ann. Biomed. Eng. 38 (3) (2010) 854–864.
[23] G. Valenza, H. Wendt, K. Kiyono, J. Hayano, E. Watanabe, Y. Yamamoto, P. Abry, R. Barbieri, Mortality prediction in severe congestive heart failure patients with multifractal point-process modeling of heartbeat dynamics, IEEE Trans. Biomed. Eng. (2018).
[24] M.U. Ahmed, D.P. Mandic, Multivariate multiscale entropy: A tool for complexity analysis of multichannel data, Phys. Rev. E 84 (6) (2011) 061918.
[25] M.U. Ahmed, D.P. Mandic, Multivariate multiscale entropy analysis, IEEE Signal Process. Lett. 19 (2) (2012) 91–94.
[26] H. Azami, J. Escudero, Refined composite multivariate generalized multiscale fuzzy entropy: A tool for complexity analysis of multichannel signals, Physica A 465 (2017) 261–276.
[27] X. Mao, P. Shang, A new method for tolerance estimation of multivariate multiscale sample entropy and its application for short-term time series, Nonlinear Dynam. (2018) 1–14.
[28] J. Runge, J. Heitzig, V. Petoukhov, J. Kurths, Escaping the curse of dimensionality in estimating multivariate transfer entropy, Phys. Rev. Lett. 108 (25) (2012) 258701.
[29] A. Porta, G. Baselli, D. Liberati, N. Montano, C. Cogliati, T. Gnecchi-Ruscone, A. Malliani, S. Cerutti, Measuring regularity by means of a corrected conditional entropy in sympathetic outflow, Biol. Cybern. 78 (1) (1998) 71–78.
[30] T. Schürmann, Bias analysis in entropy estimation, J. Phys. A: Math. Gen. 37 (27) (2004) L295.

[31] A. Porta, L. Faes, V. Bari, A. Marchi, T. Bassani, G. Nollo, N.M. Perseguini, J. Milan, V. Minatel, A. Borghi-Silva, et al., Effect of age on complexity and causality of the cardiovascular control: comparison between model-based and model-free approaches, PLoS One 9 (2) (2014) e89463.
[32] I. Vlachos, D. Kugiumtzis, Nonuniform state-space reconstruction and coupling detection, Phys. Rev. E 82 (1) (2010) 016207.
[33] L. Faes, G. Nollo, A. Porta, Information-based detection of nonlinear granger causality in multivariate processes via a nonuniform embedding technique, Phys. Rev. E 83 (5) (2011) 051112.
[34] W. Chen, Z. Wang, H. Xie, W. Yu, Characterization of surface EMG signal based on fuzzy entropy, IEEE Trans. Neural Syst. Rehabil. Eng. 15 (2) (2007) 266–272.
[35] G. Valenza, L. Citi, E.P. Scilingo, R. Barbieri, Inhomogeneous point-process entropy: An instantaneous measure of complexity in discrete systems, Phys. Rev. E 89 (5) (2014) 052803.
[36] G. Valenza, L. Citi, R. Barbieri, Estimation of instantaneous complex dynamics through lyapunov exponents: a study on heartbeat dynamics, PLoS One 9 (8) (2014) e105622.
[37] M. Staniek, K. Lehnertz, Symbolic transfer entropy, Phys. Rev. Lett. 100 (15) (2008) 158101.
[38] T. Heldt, E.B. Shim, R.D. Kamm, R.G. Mark, Computational modeling of cardiovascular response to orthostatic stress, J. Appl. Physiol. 92 (3) (2002) 1239–1254.
[39] A.L. Goldberger, L.A. Amaral, L. Glass, J.M. Hausdorff, P.C. Ivanov, R.G. Mark, J.E. Mietus, G.B. Moody, C.-K. Peng, H.E. Stanley, Physiobank, physiotoolkit, and physionet, Circulation 101 (23) (2000) e215–e220.
[40] N. Iyengar, C. Peng, R. Morin, A.L. Goldberger, L.A. Lipsitz, Age-related alterations in the fractal scaling of cardiac interbeat interval dynamics, Amer. J. Physiol.-Regul. Integr. Comp. Physiol. 271 (4) (1996) R1078–R1084.
[41] S.-D. Wu, C.-W. Wu, S.-G. Lin, K.-Y. Lee, C.-K. Peng, Analysis of complex time series using refined composite multiscale entropy, Phys. Lett. A 378 (20) (2014) 1369–1374.
[42] M. Nardelli, E.P. Scilingo, G. Valenza, Refined generalized multivariate multiscale Fuzzy entropy: A preliminary study on multichannel physiological complexity during postural changes, in: 2018 26th European Signal Processing Conference (EUSIPCO), IEEE, 2018, pp. 291–295.
[43] H. Abarbanel, Analysis of Observed Chaotic Data, Springer Science & Business Media, 2012.
[44] H. Kim, R. Eykholt, J. Salas, Nonlinear dynamics, delay times, and embedding windows, Physica D 127 (1–2) (1999) 48–60.
[45] A. Humeau-Heurtier, The multiscale entropy algorithm and its variants: A review, Entropy 17 (5) (2015) 3110–3123.
[46] S.J. Leistedt, P. Linkowski, J.P. Lanquart, J. Mietus, R.B. Davis, A.L. Goldberger, M.D. Costa, Decreased neuroautonomic complexity in men during an acute major depressive episode: analysis of heart rate dynamics, Transl. Psychiatry 1 (7) (2011) e27.
[47] G. Valenza, M. Nardelli, G. Bertschy, A. Lanata, E. Scilingo, Mood states modulate complexity in heartbeat dynamics: A multiscale entropy analysis, Europhys. Lett. 107 (1) (2014) 18003.
[48] M. Nardelli, A. Lanata, G. Bertschy, E.P. Scilingo, G. Valenza, Heartbeat complexity modulation in bipolar disorder during daytime and nighttime, Sci. Rep. 7 (1) (2017) 17920.
[49] G. Valenza, L. Citi, E.P. Scilingo, R. Barbieri, Point-process nonlinear models with laguerre and volterra expansions: instantaneous assessment of heartbeat dynamics, IEEE Trans. Signal Process. 61 (11) (2013) 2914–2926.
[50] T. Heldt, M. Oefinger, M. Hoshiyama, R. Mark, Circulatory response to passive and active changes in posture, in: Computers in Cardiology, 2003, IEEE, 2003, pp. 263–266.
[51] J. Pan, W.J. Tompkins, A real-time QRS detection algorithm, IEEE Trans. Biomed. Eng. 32 (3) (1985) 230–236.
[52] M.P. Tarvainen, J.-P. Niskanen, J.A. Lipponen, P.O. Ranta-Aho, P.A. Karjalainen, Kubios HRV–heart rate variability analysis software, Comput. Methods Programs Biomed. 113 (1) (2014) 210–220.
[53] L.E.V. Silva, R.M. Lataro, J.A. Castania, C.A.A. da Silva, J.F. Valencia, L.O. Murta Jr, H.C. Salgado, R. Fazan Jr, A. Porta, Multiscale entropy analysis of heart rate variability in heart failure, hypertensive, and sinoaortic-denervated rats: classical and refined approaches, Amer. J. Physiol.-Regul. Integr. Comp. Physiol. 311 (1) (2016) R150–R156.
[54] G. Nollo, L. Faes, A. Porta, R. Antolini, F. Ravelli, Exploring directionality in spontaneous heart period and systolic pressure variability interactions in humans: implications in the evaluation of baroreflex gain, Amer. J. Physiol.-Heart Circ. Physiol. 288 (4) (2005) H1777–H1785.
[55] M. Javorka, J. Krohova, B. Czippelova, Z. Turianikova, Z. Lazarova, K. Javorka, L. Faes, Basic cardiovascular variability signals: mutual directed interactions explored in the information domain, Physiol. Meas. 38 (5) (2017) 877.
[56] M. Orini, P. Laguna, L. Mainardi, R. Bailón, Assessment of the dynamic interactions between heart rate and arterial pressure by the cross time–frequency analysis, Physiol. Meas. 33 (3) (2012) 315.